ChemComm

ROYAL SOCIETY OF CHEMISTRY

FEATURE ARTICLE

View Article Online
View Journal



Cite this: DOI: 10.1039/d4cc06574c

# Shape-selective catalysis in cavity-type molecular sieves: cavity-controlled catalytic principle

Shushu Gao, †[ab] Fangxiu Ye, †[acd] Shutao Xu, *[acd] Yingxu Wei *[acd] and Zhongmin Liu [acd]

The methanol-to-olefins (MTO) process, driven by zeolites or molecular sieves, a cornerstone of C1 chemistry, has established a substantial pathway for generating olefin products from non-petroleum sources. Molecular sieves exhibit significant benefits in catalysis with shape selectivity due to the unique confinement environment and acidic properties, featuring their molecular sieving and confinement effects. Significantly, eight-membered ring (8-MR) and cavity-type molecular sieve catalysts, characterized by large cage volumes and restricted window openings, exhibit distinctive host–guest interactions between the cavity structure and the reactants, intermediates, and products within the confined space, thereby revealing the cavity-controlled methanol conversion principle in molecular adsorption and diffusion, intermediate formation, reaction pathway, and catalyst deactivation processes. This review mainly summarizes molecular adsorption characteristics and diffusion behavior, as well as the mechanisms of the MTO reaction and catalyst deactivation within cavity-type molecular sieves. A comprehensive introduction is provided on the variations in preferential adsorption sites and diffusion behavior of guest molecules induced by different cavity structures within cavity-type molecular sieves. Furthermore, the critical intermediate generation governed by cavity structure and the nonuniform distribution of coke species within the catalyst were also discussed. The cavity-controlled catalytic principle of the MTO reaction driven by 8-MR and cavity-type molecular sieves provides valuable insights for the modification of molecular sieve catalysts and the optimization of the MTO process and also promotes broader application of these catalysts in other C1 chemical reactions.

Received 16th December 2024,
Accepted 20th January 2025

DOI: 10.1039/d4cc06574c

rsc.li/chemcomm

[a] National Engineering Research Center of Lower-Carbon Catalysis Technology, Dalian Institute of Chemical Physics, Chinese Academy of Sciences, Dalian 116023, China
[b] Sinopec Beijing Research Institute of Chemical Industry, Beijing 100013, China
[c] State Key Laboratory of Catalysis, Dalian Institute of Chemical Physics, Chinese Academy of Sciences, Dalian 116023, China. E-mail: xushutao@dicp.ac.cn, weiyx@dicp.ac.cn
[d] University of Chinese Academy of Sciences, Beijing 100049, China
† These authors contributed equally to this work.

**Shushu Gao**

*Shushu Gao received her PhD at the Dalian Institute of Chemical Physics (DICP), Chinese Academy of Sciences (CAS), in 2020 and subsequently joined Sinopec Beijing Research Institute of Chemical Industry. In 2022, she became an associate professor. Her research interests focus on the application of solid-state nuclear magnetic resonance (ssNMR) to the structure and reaction mechanisms of solid catalysts, as well as adsorption and diffusion in porous materials.*

**Fangxiu Ye**

*Fangxiu Ye is currently pursuing her PhD at the Dalian Institute of Chemical Physics (DICP), Chinese Academy of Sciences (CAS), under the supervision of Prof. Shutao Xu. Her research interests focus on the applications of solid-state nuclear magnetic resonance (ssNMR) to molecular adsorption–diffusion in zeolite catalysis.*

# 1. Introduction

Light olefins, crucial raw materials for the production of various chemical products, such as synthetic plastics, fibers, and rubber, are primarily obtained from the thermal cracking of naphtha and are indispensable to the petrochemical industry.[1] Due to the limited availability of petroleum resources, the development of light olefin generation processes from non-petroleum resources has become a research hotspot. The methanol-to-olefins (MTO) reaction catalyzed by molecular sieves, due to its high production efficiency and the availability of methanol, is considered to be a sustainable alternative route with significant economic and environmental implications.[2–5] In 2010, DMTO technology using SAPO-34 molecular sieve catalysts, known as DMTO-I, developed by the Dalian Institute of Chemical Physics (DICP), was successfully applied in industry at Shenhua Baotou in China.[4] The second and third generations of the DMTO process (DMTO-II and DMTO-III) have also been successively developed. As of now, 18 DMTO reaction units have been operated, with a total low-carbon olefin production capacity of over 10 million tons per year.

A crucial aspect of the MTO process is the selection of an appropriate catalyst.[6,7] Molecular sieves, due to their shape selectivity, tunable acidity, and excellent hydrothermal stability, have become the core catalysts for the MTO reaction.[8,9] The molecular sieving and confinement effects of molecular sieves enable the entire MTO reaction to engage in shape-selective catalysis. Typical shape-selective catalytic properties, including reactant shape selectivity, transition state shape selectivity, and product shape selectivity, are exhibited in the MTO reaction. These properties are strongly influenced by the pore architecture of the molecular sieve catalyst, resulting in a complex reaction mechanism.[10–15] Clarifying the relationship between MTO reactions and structural characteristics of molecular sieve catalysts is essential for improving catalytic efficiency and optimizing catalysts.[7,11,16]

Cavity-type molecular sieves exhibit a notable spatial advantage, characterized by expansive cage-like structures and narrow window openings.[17,18] SAPO-34, as a typical cavity-type molecular sieve, which features a CHA topology and eight-membered ring (8-MR) pore opening, has been successfully applied in the MTO process.[4,19] Additionally, various molecular sieves featuring 8-MR windows and cavity structures, such as AEI, RHO, LEV, AFX, AFN, DDR, LTA, ERI, ITE, KFI, and RTH, are also considered as promising catalysts for methanol conversion.[18,20–24] The slight changes in the cavity structure of these molecular sieves significantly affect methanol conversion and product distribution,[17,23,25] illustrating the unique cavity-controlled catalytic principle.

The entire MTO process involves molecular adsorption and diffusion processes, the generation of intermediates, the evolution of the reaction pathway, and catalyst deactivation, forming

**Shutao Xu**

*Shutao Xu received his PhD from Dalian Institute of Chemical Physics (DICP), Chinese Academy of Sciences (CAS), in 2011. He then joined Prof. Zhongmin Liu's team at the National Engineering Research Center of Lower-Carbon Catalysis Technology, DICP, as a research assistant. He became a professor in 2017. His research interests include the various developments of solid-state nuclear magnetic resonance spectroscopy (ssNMR) methods, including in situ/operando techniques, 2D ssNMR spectroscopy, hyperpolarized (HP) $^{129}$Xe, and pulse field gradient (PFG) NMR, as well as applying these advanced NMR methods to the study of the structure, acidity, and reaction mechanism of catalytic materials.*

**Yingxu Wei**

*Yingxu Wei received her PhD from the Dalian Institute of Chemical Physics (DICP), Chinese Academy of Sciences (CAS), in 2001. During her service in DICP, she conducted her postdoctoral studies at the University of Namur (Belgium) from 2003 to 2004. She has been the group leader of Catalysis and New Catalytic Reactions in the National Engineering Laboratory of Methanol to Olefins since 2009 and was promoted to professor in 2011. Over the years, Prof. Wei has undertaken a number of key academic research projects commissioned by NSFC, CAS, MOST, PetroChina, and other organizations. She has published over 100 academic papers, and she has applied for and been granted more than 60 patents.*

**Zhongmin Liu**

*Prof. Zhongmin Liu is the Director of the Dalian Institute of Chemical Physics (DICP), Chinese Academy of Sciences (CAS), since 2017. For many years, he has been working on catalysis research, process development, and technology transfer in energy conversion and utilization, obtaining significant achievements. Prof. Liu led his team to successfully commercialize two of the most representative industrial processes, methanol to olefins (MTO) and methanol to ethanol (MTE), in 2010 and 2017, respectively, which are important advances in coal to chemicals. He has published more than 430 research papers and obtained more than 600 authorized patents.*

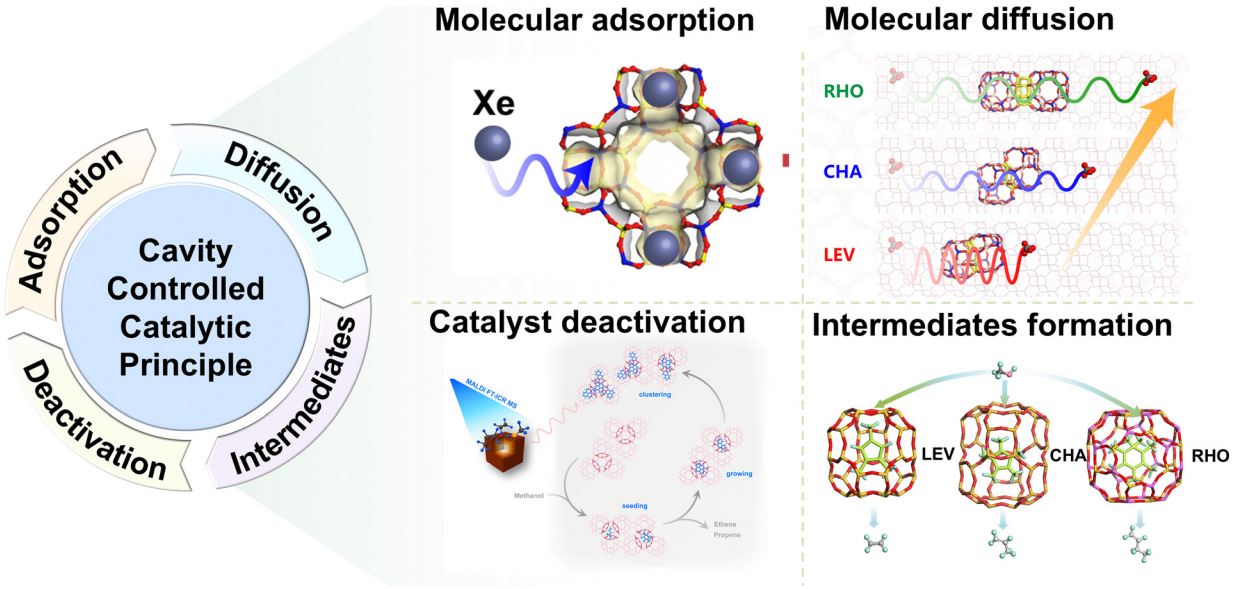


Fig. 1 Schematic representation of the cavity-controlled catalytic principle, including molecular adsorption, diffusion, critical intermediate formation, and catalyst deactivation in the MTO reaction using 8-MR and cavity-type molecular sieves.[11–15,18] This is a reprocessed figure, some of which was adapted from ref. 13 (2021), American Chemical Society; ref. 14 (2019), Elsevier; ref. 12 (2020), Springer Nature; and ref. 18 (2015), American Chemical Society.

a complex dynamic reaction network (Fig. 1). The cavity structure of the catalyst controls these key processes by the spatial confinement effects and chemical environment, which directly impact the catalytic activity and stability of the catalyst, enabling highly selective catalysis. This leads to the establishment of the cavity-controlled catalytic principle, which includes cavity-controlled adsorption and diffusion, cavity-controlled intermediate formation, and cavity-controlled coke formation. This feature article aims to introduce the impact of the cavity structure of 8-MR and cavity-type molecular sieves on these reaction processes and to elucidate the correlation between the structure features and catalytic activity in the MTO reaction.

## 2. Cavity-controlled adsorption and diffusion

The MTO process catalyzed by molecular sieves is a heterogeneous reaction. Reactant and product molecules experience multi-scale adsorption and diffusion processes, including within the catalyst bed, catalyst particles, crystals, and the pore system of the molecular sieve catalyst in the MTO catalytic process.[26] Therefore, the adsorption behavior and mass transfer processes of reactant and product molecules within catalysts are prerequisites for highly efficient catalytic reactions.[26–28] Numerous studies have shown that the microscopic features of the molecular sieve, including pore dimension, pore shape, and distribution of acidic sites, as well as the interactions between the framework and reactants, products, and intermediates in confined spaces, have a significant impact on molecular adsorption and diffusion.[29–32] This contributes to a deeper understanding of reaction mechanisms and inspires novel concepts for catalyst design.

The processes of molecular adsorption and mass transfer within molecular sieves are highly linked and serve as the foundation of the catalytic cycle. The diffusion process of molecules within pores refers to the migration of molecules between adsorption sites within the molecular sieves. The position, number, and intensity of the adsorption sites within the molecular sieve directly influence the mass transport processes of guest molecules. A thorough understanding of the adsorption features of molecules within confined spaces of cavity-type molecular sieves is essential for elucidating the diffusion mechanism. In cavity-type molecular sieves, the cages are linked either by a shared single ring or through a double ring. The adsorption features and diffusion patterns of guest molecules are significantly influenced by the dimensions of confined spaces of window units between cages. The DNL-6 molecular sieve, initially synthesized by the DICP, demonstrates catalytic performance in MTO reactions.[33] DNL-6 molecular sieve features a RHO topology with cubic symmetry. It contains *lta* cavities that are interconnected in three-dimensional directions through double eight-membered rings (D8R). Gao *et al.*[13] explored the dynamic adsorption behavior and diffusion process of xenon within the constrained environment of the *lta* cage and D8R within DNL-6 molecular sieves using pulsed field gradient (PFG) NMR, $^{129}$Xe NMR, Monte Carlo (MC), and molecular dynamics (MD) simulations, which provided a microscopic understanding of the preferential adsorption characteristics of xenon adsorbed inside RHO-type molecular sieves and the correlation between preferential adsorption features and mass transfer behavior in restricted spaces. As shown in Fig. 2, the concentration-dependent $^{129}$Xe

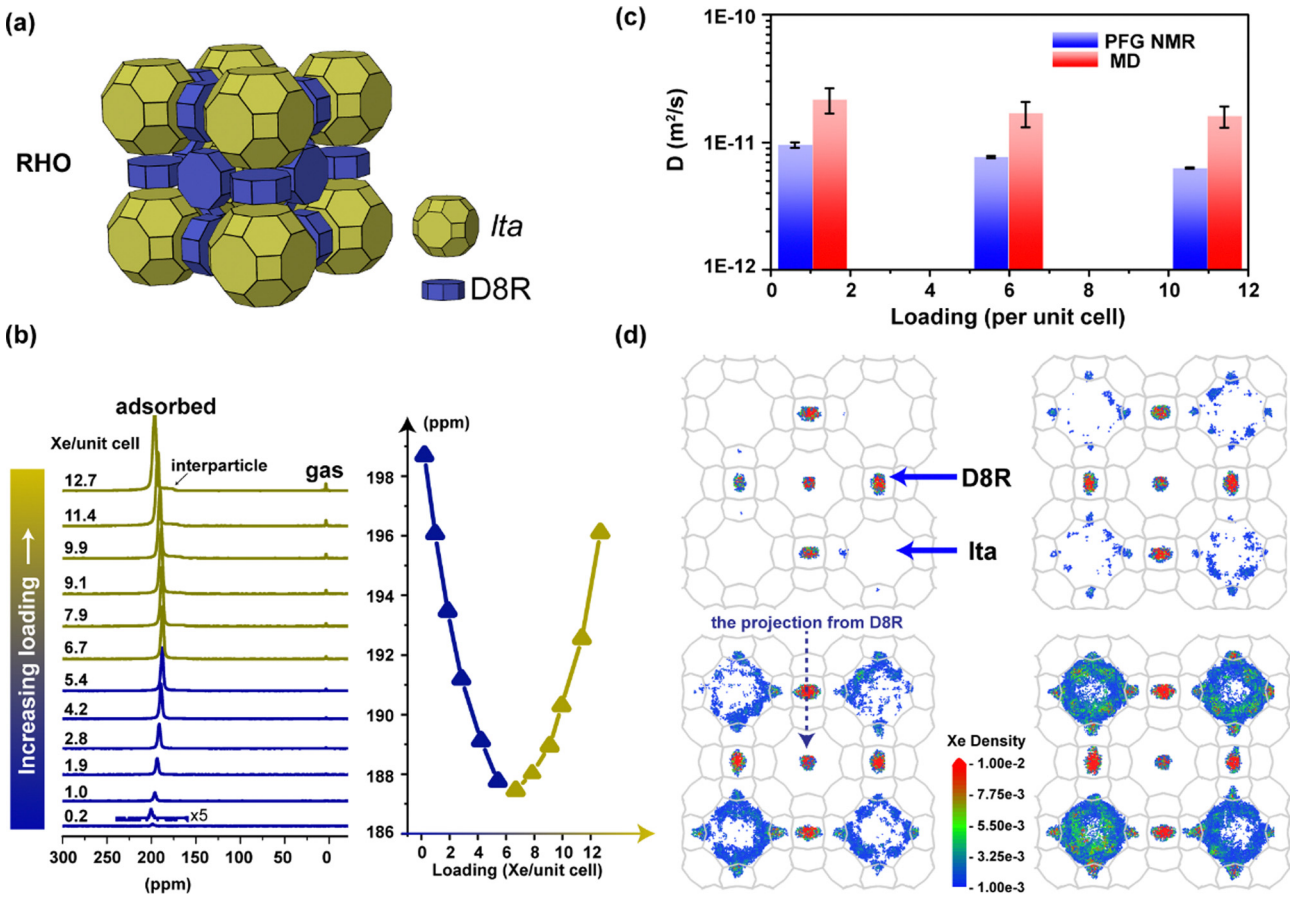


Fig. 2 The adsorption feature and diffusion behavior of xenon within DNL-6 molecular sieves with an increased xenon loading. (a) The three-dimensional structure of RHO topology. (b) $^{129}$Xe NMR spectra and $^{129}$Xe chemical shift value of adsorbed xenon inside DNL-6 at different loadings. (c) Loading-dependent xenon self-diffusion coefficients inside DNL-6 obtained from PFG NMR and MD. (d) Xenon adsorption density maps at various xenon loadings in RHO. Reproduced with permission from ref. 13. Copyright (2021) American Chemical Society.

NMR and theoretical simulation reveal the presence of distinct adsorption sites within the DNL-6 molecular sieve, with the D8R site being the most favored for xenon adsorption. As the xenon loading increases, the high density of adsorbed xenon in the D8R region contributes to the increase in residence time of xenon, resulting in enhanced diffusion limitations and a reduced overall diffusion rate of xenon adsorbed within the DNL-6 molecular sieve. In porous media, the concentration dependence of intracrystalline self-diffusion typically depends on pore structure, the interactions between molecules, the position of adsorption sites, and so on.[32,34–36] Therefore, this work demonstrates that the adsorption characteristics and transport kinetics of guest molecules in 8-MR and cavity-type molecular sieves are strongly influenced by the interactions between the pore structure and molecules, reflecting the cavity-controlled adsorption and diffusion within the molecular sieve.

Further investigation was conducted on the spatial confinement effect of D8R in RHO molecular sieve on reactant methanol in the research of Lou *et al.* using solid-state NMR (ssNMR) technique and theoretical simulation,[37] particularly on the orientation of methanol adsorption within the cavity structure. A detailed investigation into the adsorption behavior of methanol molecules within distinct spatial confinement environments was performed, using the DNL-6 and SAPO-42 molecular sieves with similar cage structures, as shown in Fig. 3. Unlike the DNL-6 molecular sieve, the SAPO-42 molecular sieve has an LTA topology, where *lta* cavities are linked through a single 8-MR window rather than the D8R. $^{13}$C MAS NMR spectra of methanol adsorption on DNL-6 and SAPO-42 molecular sieves show that the adsorption behavior of methanol varies in the cage structures of different molecular sieves. Compared to the single 8-MR window of LTA topology for the SAPO-42 molecular sieve, the D8R environment in the DNL-6 exhibits a stronger spatial confinement effect on methanol adsorption, which leads to the high $^{13}$C chemical shift values of methanol molecules and a stronger orientation of methanol molecules within the molecular sieve. The orientation of methanol molecules during adsorption within the DNL-6 molecular sieve at the low loading is characterized by the most energetically favorable arrangement and also exhibits the largest $^{13}$C chemical shift, where the methyl group of methanol is directed towards the D8R confined region and the hydroxyl groups are stabilized by the Brønsted acid sites (BASs). Additionally, the interaction between acidic sites of molecular sieves and

 

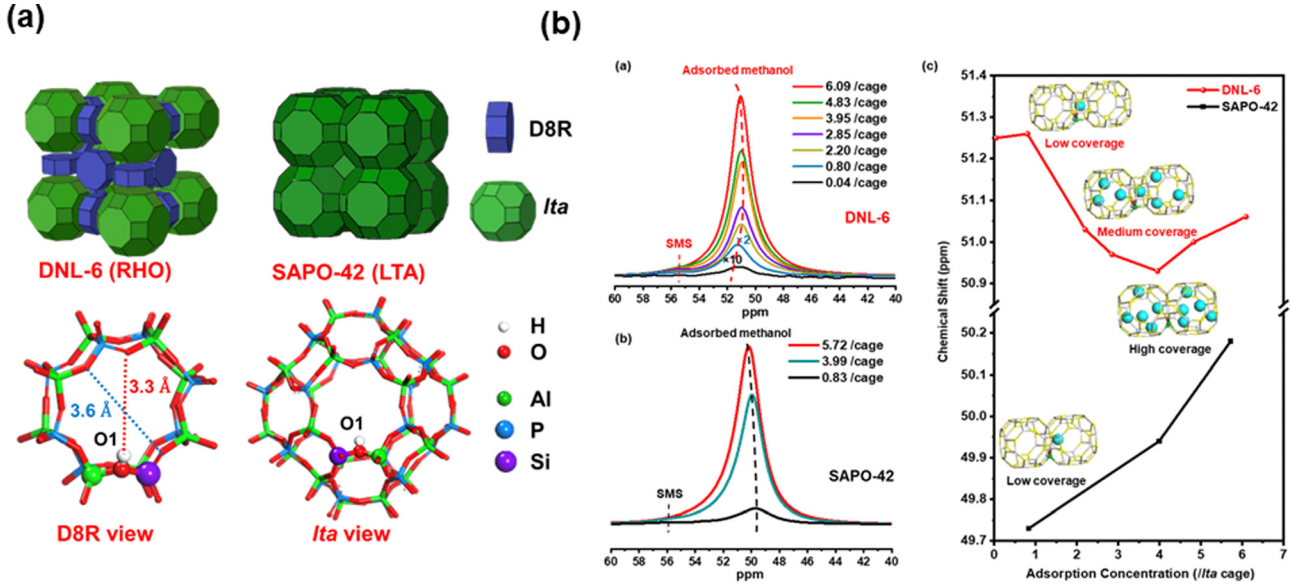


Fig. 3 Loading-dependent methanol adsorption in DNL-6 and SAPO-42 molecular sieves, respectively. (a) The three-dimensional structure and optimized structures of BASs in RHO and LTA topologies, respectively. (b) $^{13}$C MAS NMR spectra and corresponding $^{13}$C chemical shift values of $^{13}$C-methanol within DNL-6 and SAPO-42 molecular sieves with various loadings, respectively. Reproduced with permission from ref. 37. Copyright (2021) Wiley-VCH.

adsorbates may influence molecular adsorption behavior. Studies show that the strength and distribution of BASs in SAPO molecular sieves also play a key role in methanol adsorption behavior. For SAPO-42, the presence of a single BAS and *lta* cavity creates specific adsorption sites for methanol. For DNL-6, the acid site O1 exhibits stronger acidity than O2 due to its lower deprotonation energy, resulting in the preferred adsorption of methanol molecules at the O1 acid site. However, the differences in methanol adsorption stability are primarily caused by the D8R confined environment rather than variations in the acid sites. The adsorption energy of methanol molecules for the D8R orientation is 4.4–5.3 kJ mol$^{-1}$ lower than that of the *lta* cage orientation, and the predicted chemical shifts for the D8R orientation are approximately 1.0 ppm higher than that of *lta* cage orientation. The confined space of D8R works synergistically with the BAS, enhancing both the adsorption capacity and the molecular orientation of methanol. This finding highlights the critical role of the spatial confinement arising from cage structure in the selective adsorption of molecular sieves and provides new insights into the understanding of catalytic reaction mechanisms.

Moreover, the heterogeneity of adsorption behavior of guest xenon atoms adsorbed inside individual SAPO-34 crystals was explored by Gao *et al.*[38] The finding revealed a gradient distribution of xenon adsorption within individual SAPO-34 crystals and proposed a multi-layer adsorption model for xenon clusters of varying sizes at the single-crystal scale, as shown in Fig. 4. On an individual SAPO-34 crystal, xenon clusters, denoted as $Xe_n$ ($n$ = 2–5), are distributed in decreasing size from the surface to the interior of the crystals. The formation of such xenon clusters is closely related to the unique cavity structure of SAPO-34. The spatial confinement effect of the cavity structure encourages xenon atoms to aggregate into xenon clusters. The spacious cage volume provides sufficient space for the formation of larger xenon clusters, while the narrow 8-MR windows limit the rapid exchange of these xenon clusters between different cages, leading to the heterogeneity of xenon adsorption inside the cages. This non-uniform adsorption distribution notably influences both adsorption kinetics and the mass transfer process. Quantitative analysis of the xenon self-diffusion coefficient within SAPO-34 molecular sieves revealed a faster xenon diffusion near the crystal surface, which is associated with the higher xenon adsorption loading in this region. The change in molecular diffusion behavior resulting from the non-uniform adsorption, especially for the diffusion of reactant methanol in the MTO reaction, is crucial for catalytic reaction activity. The methanol adsorbed on the crystal surface of the catalyst with higher adsorption loading may exhibit faster diffusion rates. However, intracrystalline diffusion limitations lead to reduced efficiency in the diffusion of methanol to the acidic sites located at the interior of the crystal. This results in local accumulation of reactants, which can promote secondary reactions and ultimately accelerate catalyst deactivation. Moreover, this diffusion behavior of methanol may also affect the product selectivity. Additionally, this multi-layer adsorption model was used for studying the heterogeneity of the MTO reaction and deactivation processes at a microscopic level, particularly the presence of the surface barrier or internal diffusion resistance arising from the surface composition or internal intergrowth, which also offers important perspectives on the correlation between adsorption features, mass transfer processes, and catalyst deactivation during the MTO catalysis.

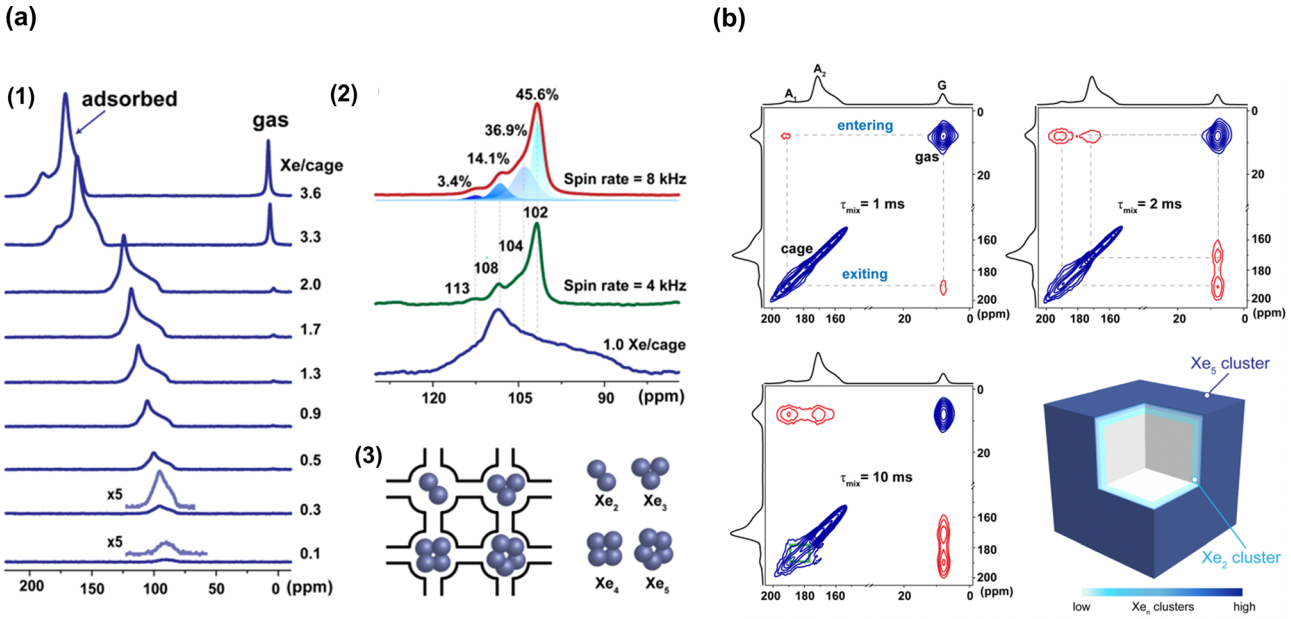


Fig. 4 The inhomogeneous distribution of the $Xe_n$ cluster in the SAPO-34 crystal. (a) Concentration-dependent $^{129}Xe$ NMR, $^{129}Xe$ MAS NMR, and corresponding static spectra, the possible structure of $Xe_n$ clusters for xenon inside SAPO-34. (b) 2D $^{129}Xe$ EXSY NMR of xenon adsorbed in SAPO-34 crystal with different mixing times and spatial distributions of $Xe_n$ clusters located within an individual SAPO-34 crystal. Reproduced with permission from ref. 38. Copyright (2019) Royal Society of Chemistry.

Molecular diffusion processes within molecular sieves are critical in governing reaction kinetics of molecules, as the rate of molecular migration impacts both the reaction speed and the distribution of products within the catalyst.[39] When the diffusion of molecules within the catalyst is restricted, the catalytic efficiency may decline, which could eventually result in catalyst deactivation.[40–42] The 8-MR window enables the passage of light hydrocarbons and restricts the mass transport of larger hydrocarbons, leading to product shape selectivity.[11] At a macroscopic scale, reducing the diffusion path (by decreasing particle size) or fabricating mesoporous or hierarchical porous molecular sieve materials are effective strategies to alleviate diffusion limitations.[43–49] At a microscopic scale, the pore channels of molecular sieves are considered as a microreactor for catalytic reactions and offer passage for mass transport of reactants and products.[13,31,37,50,51] Molecular diffusion behavior within the micropores of the molecular sieve is configurational diffusion, as the dimensions of molecules are typically comparable to the pore size.[52,53] Consequently, the pores of molecular sieves allow only molecules with specific sizes and shapes to pass through. Even small changes in the pore size could alter the molecular diffusion rate and path within molecular sieve materials.[11,14,54] The mass transfer of probe alkane molecules (methane, ethane, and propane) within 8-MR and cavity-type molecular sieves (SAPO-35, SAPO-34, and DNL-6) was investigated by Gao *et al.*[14] through the $^1H$ PFG NMR technique and theoretical simulations, and the critical role of the cage structure in the molecular diffusion process is revealed in detail at the microscopic level. Despite the similar 8-MR window opening, the mass transfer characteristics of alkane molecules depend on the cage size. The results show that the diffusion coefficient of alkanes increases with cage sizes increasing for cavity-type molecular sieves with similar 8-MR windows. As shown in Fig. 5, DNL-6 exhibits the highest self-diffusion coefficient, followed by SAPO-34, and then SAPO-35. Methane exhibits the lowest diffusion activation energy and the fastest diffusion in the DNL-6 molecular sieve with a larger cavity dimension, indicating the weakest intracrystalline diffusion limitation by the cage structure. Conversely, the small cage size of SAPO-35 imposes a more significant diffusion limitation on methane, leading to the highest activation energy for intracrystalline diffusion and the lowest intracrystalline diffusion coefficient. The relationship between cavity structure and molecular diffusion features was presented by MD simulations and a continuous-time random-walk (CTRW) coarse graining approach. The inter-cavity hopping behavior of adsorbed methane within cavity-type molecular sieves is quantitatively characterized by two essential parameters of jump frequency ($f$) and jump length ($L$). The results demonstrate that the mass transport process of molecules inside cavity-type molecular sieves is strongly influenced by the structure and size of the cage. The jump frequency is governed by cage structure, and jump length is dependent on the cage size. In the LEV structure, the energy barrier for methane to pass through the 8-MR window is the highest, leading to the lowest jump frequency. In contrast, the CHA and RHO structures exhibit lower energy barriers for inter-cage hopping of methane and higher jump frequencies. During the inter-cavity hopping process, a larger cavity results in a longer jump length. Based on this finding, a cavity-controlled diffusion mechanism within 8-MR and cavity-type molecular sieves was proposed. Research on molecular adsorption features and mass transfer properties in cavity-type

 

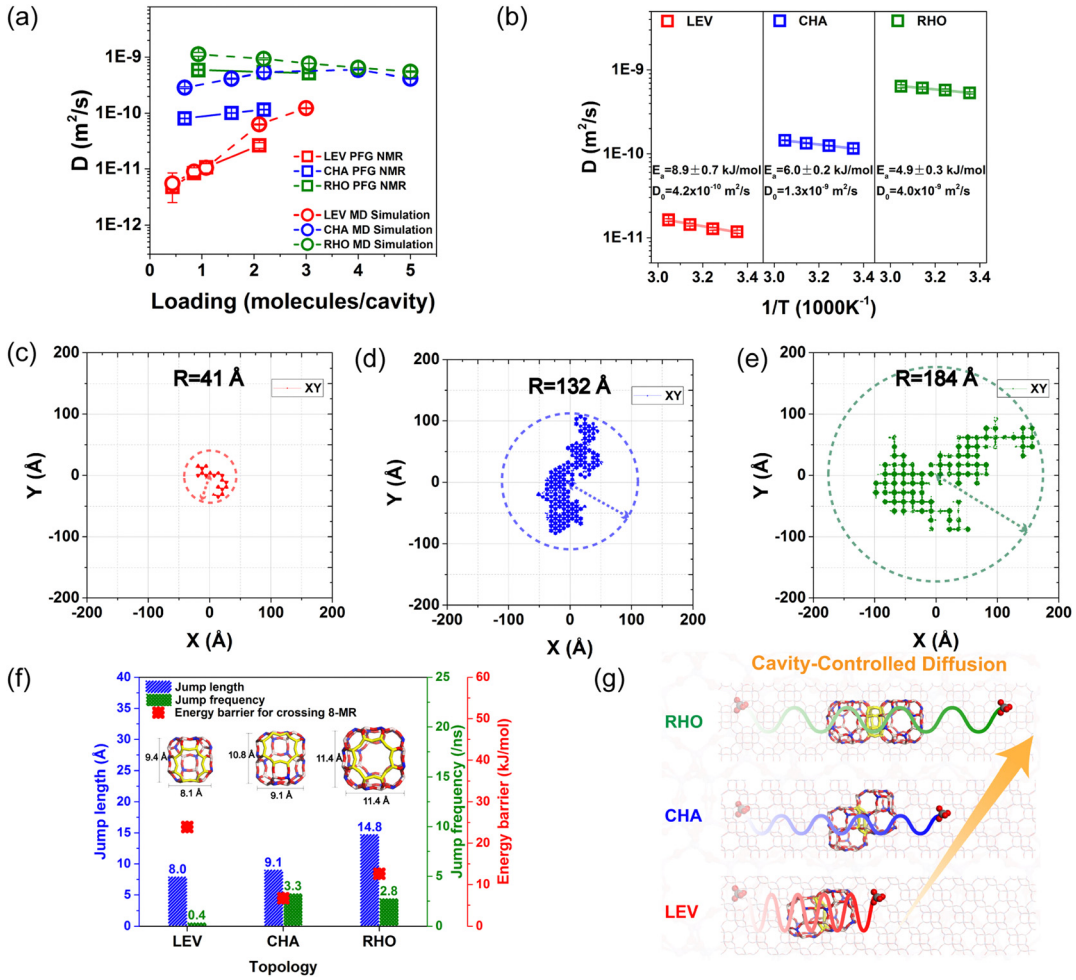


Fig. 5 Diffusion features of methane inside cavity-type molecular sieves. (a) Loading-dependent self-diffusion coefficient of methane obtained from PFG NMR and MD inside LEV, CHA, and RHO. (b) Temperature-dependent self-diffusion coefficients and corresponding activation energies for methane diffusion inside LEV, CHA, and RHO. (c)–(e) Diffusion trajectories of methane LEV (c), CHA (d), and RHO (e) in the XY plane. (f) Jump frequency (*f*), jump length (*L*), and the energy barrier required for molecules to pass through the 8-MR window in LEV, CHA, and RHO. (g) Schematic illustration of diffusion controlled by the cavity structure. Reproduced with permission from ref. 14. Copyright (2019) Elsevier.

molecular sieves highlights the crucial impact of confined spaces on the dynamic characteristics of guest molecules and provides deeper insights into improving reaction control strategies for cavity-type molecular sieves and the understanding of the mechanism of shape-selective catalysis in the MTO process.

Furthermore, grasping the diffusion properties of molecules within the confined environment of cavity-type molecular sieves is essential for developing and optimizing high-performance molecular sieve catalysts. In the MTO process, product selectivity can be regulated by enhanced intracrystalline diffusion limitation through the modification of cavity-type molecular sieve catalysts with metal cations. Zhong *et al.*[55–57] proposed a strategy to enhance ethylene selectivity by modifying SAPO-34 catalysts with zinc ions and increasing diffusion resistance in the MTO conversion. Zinc ion modification facilitated the generation of a unique core–shell structure in the SAPO-34 catalyst, with zinc ions primarily distributed in the outer shell layer of the SAPO-34 crystal.[55] This modification not only altered the acidity of the catalyst but also contributed to the increase in diffusion limitation for large hydrocarbon products. The increased diffusion restrictions facilitated a significant improvement in ethylene selectivity during the initial MTO reaction stages.

## 3. Cavity-controlled intermediate formation

The conversion process of methanol to light olefins using a molecular sieve catalyst involves three key stages: the induction stage, the steady-state stage, and the deactivation stage.[58–67] In the initial stage, methanol undergoes a direct reaction mechanism that triggers the formation of the first C–C bond.[64–67] Many direct mechanisms have been proposed, such as free radicals, carbenes, oxonium ylides, and methane–formaldehyde (FA).[64,65,67,68] In a CHA-type molecular sieve, *in situ* DRIFT and $^{13}$C NMR spectroscopy, combined with theoretical calculation results, demonstrated that the surface methoxy species

(SMS), assisted by framework oxygen of the molecular sieve, could synergistically drive the methanol or DME conversion reaction.[67] This process enables the creation of the first C–C bond, which is followed by the production of ethene or propene. In the steady-state stage, the autocatalytic process of the MTO reaction is driven by the hydrocarbon pool (HCP) mechanism, where the zeolite and confined organic species act as the catalyst.[63,69] Identifying and capturing these active HCP species contributes to understanding the HCP mechanism during the autocatalytic stage. The narrow 8-MR window and cavity-type structure of molecular sieves offer a structural basis for their efficient MTO catalytic performance.[23,27,33] During methanol conversion catalyzed by 8-MR molecular sieves with a cavity-type structure, the spatial confinement of the cage structure can have a pronounced impact on the generation of important intermediates.[70,71] The formation of the key intermediates is strongly influenced by the cage dimensions of molecular sieves. A larger cage structure can accommodate larger active aromatic intermediates, facilitating the aromatic-mediated catalytic cycle.[18,33,71,72] Studies on the catalytic performance of 8-MR SAPO molecular sieves in the MTO reaction with a similar acid strength show that the product distribution varies due to differences in the dimension of the cage structure.[23] For the MTO reaction catalyzed by SAPO-35 with LEV topology, the main products are ethene and propene. However, for SAPO-18 (AEI) and SAPO-34 (CHA), which have larger cage sizes, propylene and butylene are the predominant products. In the deactivation period, the heavier aromatic species in confined spaces of an 8-MR molecular sieve, referred to as coke, are unable to diffuse out of the 8-MR window, resulting in catalyst deactivation by either covering the active sites or blocking the pore channel. Therefore, the cavity-type structure of 8-MR molecular sieves plays a key role in critical intermediate formation, reaction pathways, and catalyst deactivation.[10,12,18,21] The interactions between the cavity-type structure of molecular sieves and reactants, products, or intermediates dictate the selectivity of the target products or reaction paths, achieving shape-selective catalysis.

Studies have shown that the cavity-type structure of 8-MR molecular sieves creates a more favorable chemical microenvironment for the formation of key intermediates and further controls product selectivity.[18,21,73] SAPO-34 and SSZ-13, both exhibiting CHA topology but with different compositions, serve as crucial MTO catalysts. Research by Xu *et al.* indicated that in the MTO reaction, heptamethylbenzenium cation (heptaMB$^+$) and pentamethylcyclopentadienium cation (pentaMCP$^+$) were both detected on SSZ-13 due to stronger acid strength, and only pentaMCP$^+$ was identified on SAPO-34, as identified by $^{13}$C MAS NMR (Fig. 6).[15] The pentaMCP$^+$ and heptaMB$^+$ are involved in the MTO process by the paring and side-chain mechanism, respectively, demonstrating distinct activities on two CHA-type zeolites.

Furthermore, the critical intermediate species, trimethylcyclopentadienium cations (triMCP$^+$) and tri/tetramethylbenzenium cations (tri-/tetraMB$^+$), characterized by fewer methyl groups, were identified by Zhang *et al.* in the cavity-type

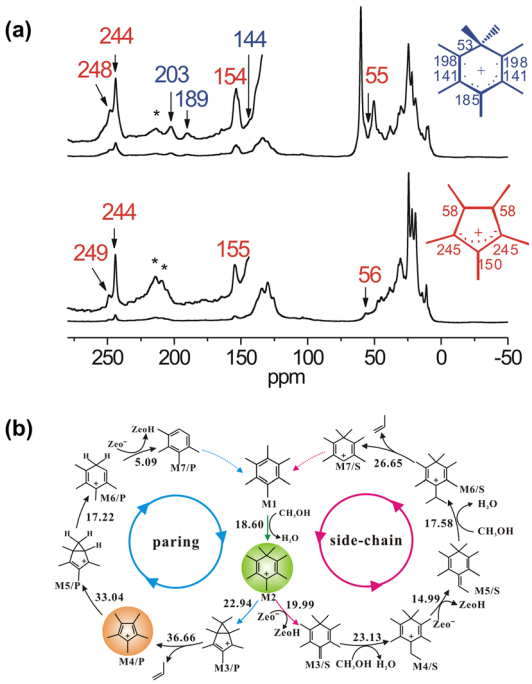


Fig. 6 The key intermediates and involved reaction pathway during the MTO reaction using SAPO-34 and SSZ-13. (a) $^{13}$C MAS NMR spectra of the confined key intermediates formed in SAPO-34 (top) and SSZ-13 (bottom) after methanol conversion. (b) Catalytic cycles of the paring and side-chain methylation mechanisms for the MTO reaction over SSZ-13 zeolite. Reproduced with permission from ref. 15. Copyright (2013) Wiley-VCH.

H-RUB-50 molecular sieve with LEV topology in the MTO reaction.[17] As shown in Fig. 7, it indicates that the spatial restriction effect induced by the cavity structure is essential for the generation and stabilization of these smaller-sized reaction intermediates. Based on the identification of intermediate species, the formation processes of ethene and propene in the MTO reaction catalyzed by the H-RUB-50 molecular sieve were predicted. The DFT result indicates that the side-chain methylation mechanism serves as the pivotal pathway for ethene generation. It was found that the generation of olefin precursors is a key step in determining product selectivity. The free energy barrier for 3,4,5-trimethyl-1-propylbenzenium (TMPB$^+$) of the propylene precursor is 36.43 kcal mol$^{-1}$, which is higher than that of the 3,4,5-trimethyl-1-ethylbenzenium (TMEB$^+$) of the ethylene precursor at 23.15 kcal mol$^{-1}$. This provides support for the preferential production of ethene on H-RUB-50.

Moreover, a detailed investigation of the influence of cage structures on the formation of key intermediates and olefin generation during the MTO reaction using 8-MR and cavity-type molecular sieves was performed. A catalytic principle of cavity-controlled MTO reactions and olefin product generation was proposed. Li *et al.*[18] explored the effect of cage structures of 8-MR SAPO molecular sieves with varying cavity dimensions (SAPO-34, SAPO-35, and DNL-6 molecular sieves) on the generation of key intermediates, methanol conversion, and distribution of olefin products in the MTO reaction (Fig. 8). The

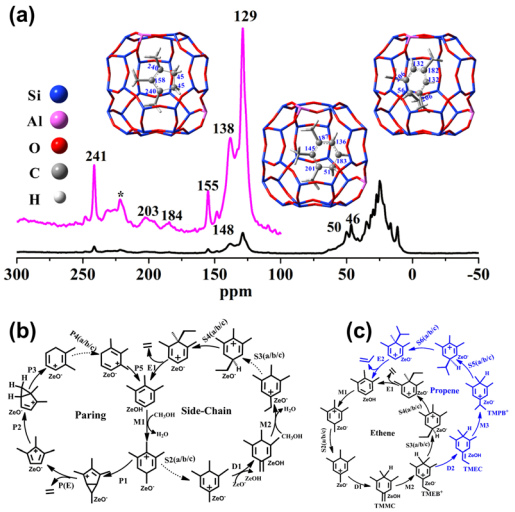


Fig. 7 The intermediate formation and reactions pathway within the confined space of H-RUB-50. (a) $^{13}$C MAS NMR spectrum of confined key intermediates formed inside H-RUB-50. (b) Catalytic cycles of the paring and side-chain methylation mechanisms for ethene generation over H-RUB-50. (c) Catalytic cycles of side-chain methylation mechanism for the generation of ethene and propene on H-RUB-50. Reproduced with permission from ref. 17. Copyright (2018) American Chemical Society.

reactivity and key role of intermediates in olefin production were confirmed. It is demonstrated that the confinement effect of the cage structure significantly influences the formation and reactivity of intermediates and further regulates the MTO catalytic activity and the distribution of olefin products. It is shown that polymethylbenzenium cation (polyMB$^+$) and ploymethylcyclopentadienium cation (polyMCP$^+$) are critical intermediates identified within three SAPO molecular sieves, and the amount of methyl groups and the reactivity of these key intermediates depend on the cage size due to spatial confinement. The smaller the cage size, the fewer the methyl substituents on the carbonium cations or the smaller the molecular size. In the DNL-6 molecular sieve with a larger cage size, larger carbonium cations such as pentaMCP$^+$ and heptaMB$^+$ are formed. triMCP$^+$, tetramethylcyclopentadienium cations (tetraMCP$^+$), and pentaMCP$^+$ were detected on SAPO-34. In SAPO-35, triMCP$^+$, tetraMCP$^+$, and pentamethylbenzenium cation (pentaMB$^+$) were identified. Finally, the olefin products distribution exhibits different features in the MTO reaction. In DNL-6 molecular sieve, which has the largest cage size, butenes are the predominant products. For SAPO-34, with a relatively large cavity size, the primary olefin products are propene and ethene. For the SAPO-35 molecular sieve, characterized by the smallest cage size, ethene is the dominant olefin product. This finding highlights the critical role of the cage structure of 8-MR molecular sieves and provides theoretical insights for the control strategy of olefin selectivity.

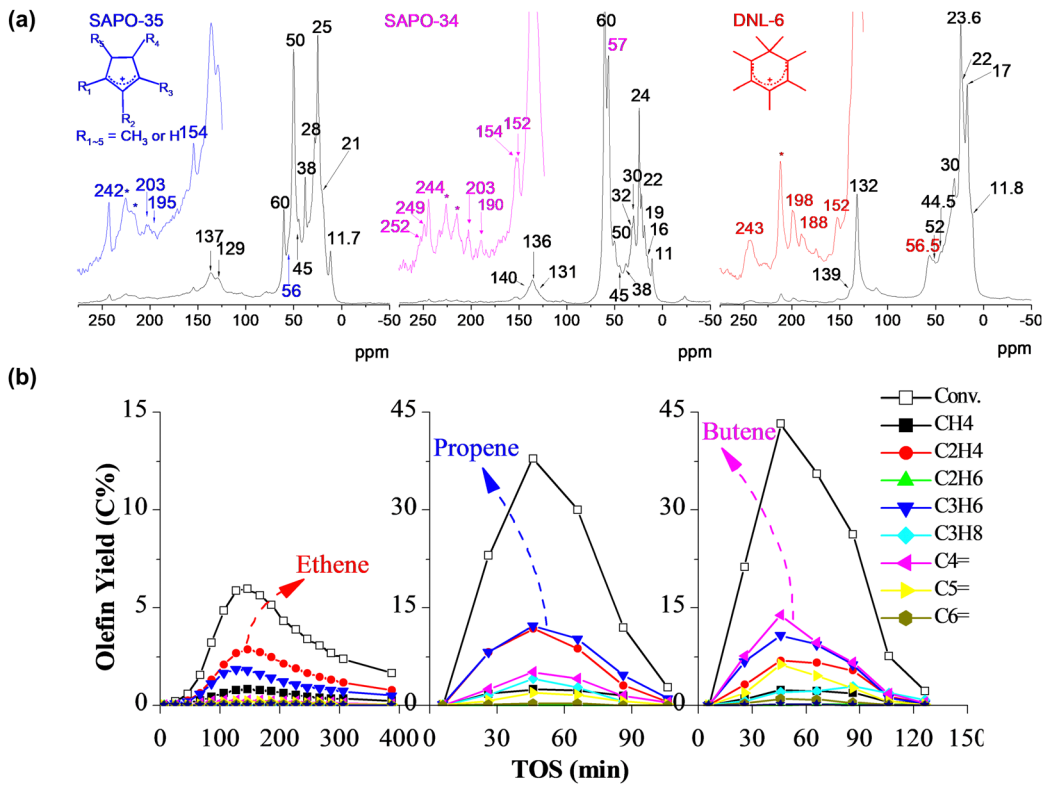


Fig. 8 The key intermediate formation and product distribution on DNL-6, SAPO-34, and SAPO-35 cavity-type molecular sieves. (a) $^{13}$C MAS NMR spectra of confined species in three molecular sieve catalysts after $^{13}$C-methanol conversion. (b) Methanol conversion and olefin production yields using SAPO-35 (left), SAPO-34 (middle), and DNL-6 (right) in the MTO reaction. Reproduced with permission from ref. 18. Copyright (2015) American Chemical Society.

As MTO catalysts, the cavity-type structure of 8-MR molecular sieve catalysts is critical in the generation of key intermediates and the determination of reaction pathways involving these intermediates. Moreover, the significant effect of cavity-type structure on molecular diffusion also improves comprehension of the cavity-controlled catalytic principle on reaction mechanism, presenting shape selectivity in the MTO reaction, as shown in Fig. 9. Therefore, the cavity-controlled shape-selective catalysis principle, including cavity-controlled intermediate formation, cavity-controlled reaction paths, and cavity-controlled diffusion, enables high selectivity of 8-MR and cavity-type molecular sieves in catalytic reactions and also provides a scientific basis for the design and optimization of catalysts.

## 4. Cavity-controlled coke formation

For 8-MR and cavity-type molecular sieves, the mass transfer restrictions imposed by the narrow 8-MR window lead to the formation and accumulation of non-reactive polycyclic aromatic hydrocarbons during methanol conversion. These non-reactive polycyclic aromatic hydrocarbons are the primary coke species.[11,12,74] These coke species can cover the active centers and obstruct pore openings and occupy cage structures of the catalyst, which restricts the transport of reactants and products and prevents methanol from accessing the active centers, leading to catalyst deactivation.[27]

In the MTO process, a nonuniform spatial location of coke species has been observed on the SAPO-34 catalyst.[62,75,76] The inhomogeneity in adsorption and reaction, caused by the pore structure, crystal size, and distribution of acidic sites of molecular sieves, results in the formation and accumulation of coke in specific regions, which affects the activity and lifetime of the catalyst.[12,71,77,78] Gao *et al.*[75] studied the deactivation process of the MTO reaction using the SAPO-34 catalyst, focusing on the formation and spatial location of coke within SAPO-34 and its impact on mass transfer performance and accessibility to acidic sites during the MTO reaction. Coke formation exhibits a nonuniform distribution within the SAPO-34 crystals, and coke species are predominantly positioned in the external layer of the crystals, as shown in Fig. 10. This distribution leads to significant mass transfer limitations within the catalyst. The intracrystalline diffusion coefficients of methane and ethene adsorbed within SAPO-34 decrease significantly as coke amount increases, respectively. Moreover, this heterogeneous distribution of coke results in many acidic sites within the SAPO-34 crystal remaining inaccessible to reactants due to coke coverage, contributing to a marked reduction in catalytic activity. This study highlights the key role of the formation and spatial distribution of coke in molecular mass transfer within the catalyst and also offers insight into the understanding of nonuniform coke distribution resulting from the nonuniform adsorption and diffusion of molecules in the SAPO-34 molecular sieve. This finding is also of great significance for catalyst optimization. By decreasing the crystal size or altering the distribution of acid sites, the nonuniform distribution of coke formation can be alleviated, and catalyst activity and lifetime can be improved.[79–81]

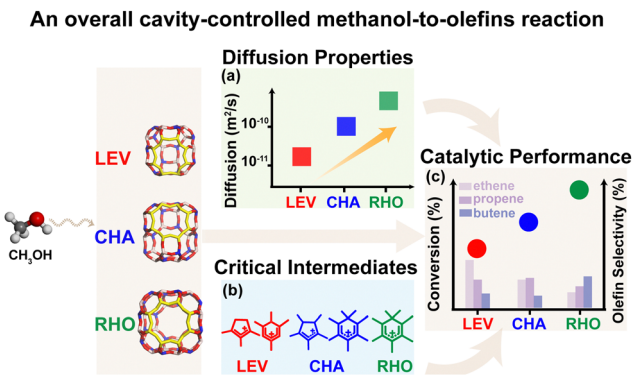


Fig. 9 Cavity-controlled MTO conversion on 8-MR and cavity-type molecular sieves. Reproduced with permission from ref. 14. Copyright (2019) Elsevier.

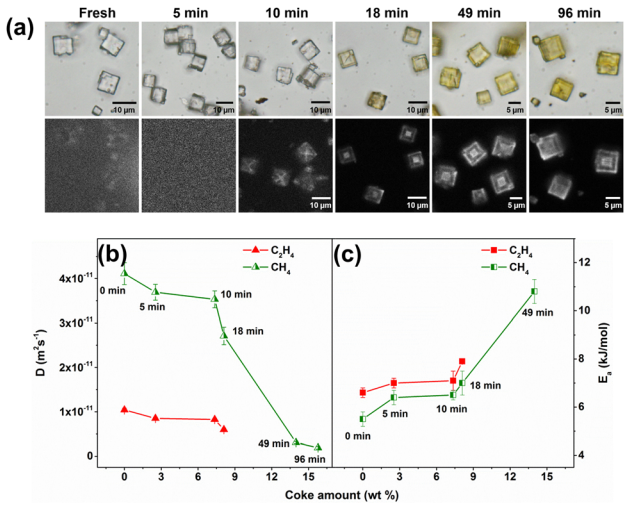


Fig. 10 The coke location and molecular diffusion behavior in the MTO process catalyzed by the SAPO-34 catalyst. (a) Confocal fluorescence microscopy (CFM) and bright field images of SAPO-34 crystals at various MTO reaction times. (b) The self-diffusion coefficient and (c) diffusion activation energies of methane and ethylene within the SAPO-34 catalyst with different coke amounts, respectively. Reproduced with permission from ref. 75. Copyright (2018) Elsevier.

Furthermore, to clarify the effect of the confined environment of the 8-MR molecular sieve with cavity structure on the generation of coke species during the MTO process, Wang *et al.*[12] identified the molecular structures of heavy polycyclic aromatic hydrocarbons (PAHs) at the molecular level and proposed the evolutionary pathway of PAHs in cavity-type SAPO-34 molecular sieve using matrix-assisted laser desorption/ionization Fourier-transform ion cyclotron resonance mass spectrometry (MALDI FT-ICR MS) and isotope labeling techniques. As shown in Fig. 11, the study demonstrated that PAH molecules grow across adjacent cage structures *via* a cage-passing growth mechanism. The formation of three-dimensional cross-linked multicore aromatic with a graphene-like structure was proposed for the first time. The

 

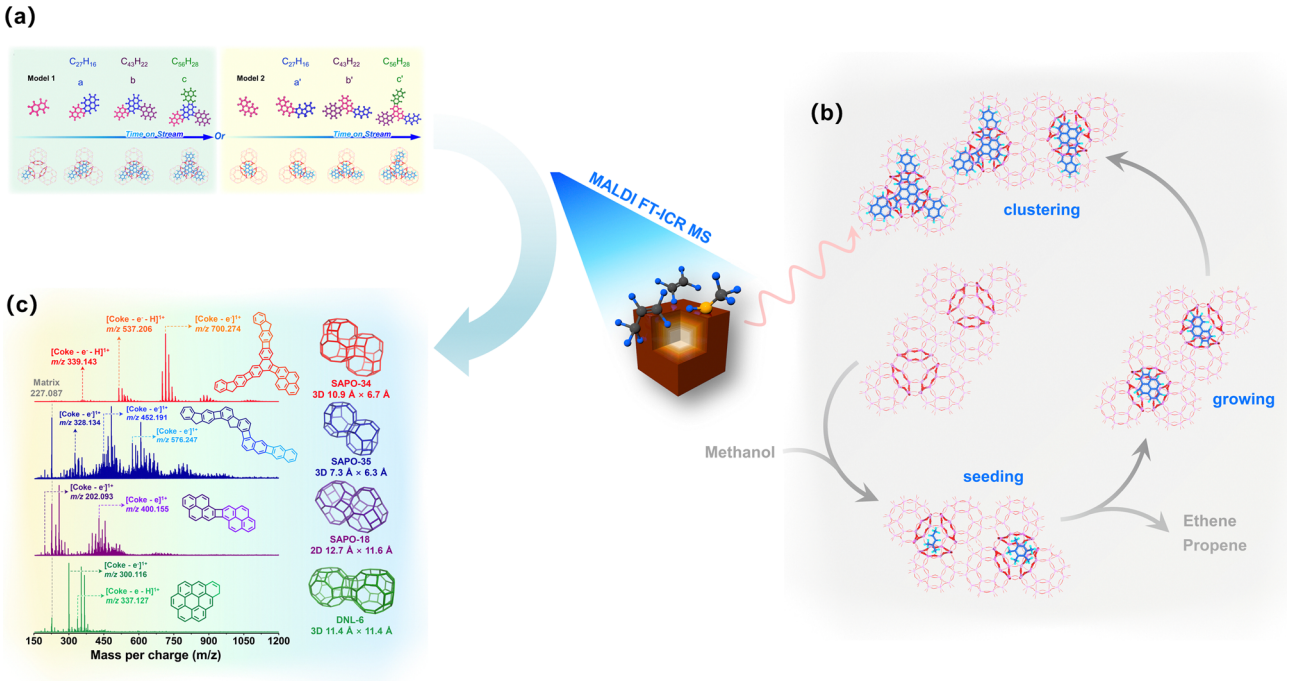


Fig. 11 The cage-passing growth of PAHs in the SAPO-34 molecular sieve. (a) The optimized possible structures of PAHs by periodic DFT calculation and their evolution pathways. (b) Schematic diagram of evolution pathways of PAHs. (c) MALDI FT-ICR mass spectra and possible molecular structure of PAHs within cavity-type molecular sieves. Reproduced with permission from ref. 12. Copyright (2020) Springer Nature.

cage-passing growth mechanism was also confirmed in other molecular sieves with cavity structure, such as SAPO-35 and SAPO-18 with cage structure connected by a single 8-MR. However, for the DNL-6 molecular sieve with a cage structure connected by a double 8-MR, no cage-passing events were observed due to the cage-passing coupling of the coke building unit being hindered by the longer distance between double 8-MR. This work offers new insights into the catalyst deactivation mechanism and provides strategies to address catalyst deactivation issues in industrial MTO processes, especially in the application of pre-coking and partial regeneration technologies. Furthermore, a detailed spatial distribution model for coke within individual catalyst crystals was presented, showing that cross-linked multicore aromatics preferentially accumulate in the outer layer of SAPO-34 crystals.

## 5. Conclusion and outlook

The MTO process has garnered significant success in industrial applications due to the highly shape-selective capabilities of molecular sieves. Advanced studies on shape-selective catalytic mechanisms not only enhance the understanding of catalytic processes but also provide essential theoretical insights and practical guidance for the creation of new catalyst materials and the improvement of industrial operating conditions. 8-MR and cavity-type molecular sieves with their narrow 8-MR openings and cavity structures exhibit unique shape selectivity in MTO applications and achieve high catalytic selectivity by precisely controlling the adsorption behavior and mass transfer processes of reactants and products, the generation of key intermediates, and the dominant reaction pathways involving these intermediates within the reaction network and catalyst deactivation in the MTO catalysis. This article mainly summarizes the crucial role played by the cage structure of 8-MR molecular sieves in molecular adsorption, mass transfer, catalytic reactions, and catalyst deactivation. The spatial confinement effect of the cage structure not only affects the molecular selective adsorption but also significantly controls the diffusion pathways and rates of molecules. Moreover, the formation of key intermediates and corresponding reaction pathways of these intermediates and catalyst deactivation were governed by cage structure, leading to product selectivity. The principles of cavity-controlled shape-selective catalysis for the MTO process were emphasized. These studies have important theoretical guidance significance for MTO reaction catalysts and process optimization.

Moreover, these studies also highlight the significance of *in situ* measurements of adsorption and diffusion processes for molecules within molecular sieve catalysts during real catalytic reactions, which are crucial for the understanding of reaction mechanisms. The diffusion process of molecules within the pores of catalysts plays a crucial role in determining reaction pathways and product distribution. Especially for multi-component reaction systems under high-temperature conditions, the ability to measure molecular adsorption features and diffusion processes under *in situ* reactions is essential for elucidating reaction mechanisms and optimizing catalytic processes. Importantly, this progress is also dependent on the advancements in analytical characterization techniques. The

PFG NMR technique, as a powerful tool for accurately measuring molecular diffusion within the pores of catalysts, provides critical diffusion data for understanding the diffusion-limited effects in catalytic processes. In addition, diffusion measurements of multi-component systems, particularly using MAS PFG NMR, allow for the simultaneous monitoring of the diffusion behavior of various species. This is key for exploring reaction mechanisms in multi-component systems, especially the effects of multi-species diffusion. The *in situ* high-temperature diffusion coefficient measurements in multi-component systems using PFG NMR are especially promising and are mainly dependent on the advancement of analytical techniques. Therefore, the pivotal role of adsorption and diffusion processes in catalytic reactions should be emphasized in future research. Specifically, the application of advanced NMR techniques such as *in situ* continuous-flow NMR, PFG NMR, MAS PFG NMR, and $^{129}$Xe NMR will allow for a deeper understanding of the interplay between catalytic activity and the adsorption and diffusion of reactants and products. Furthermore, understanding the MTO reaction mechanism will increasingly depend on the combination of advanced *in situ* characterization techniques with theoretical calculation methods, which will provide deeper insights into the reaction pathway, active centers of the catalyst, and reaction kinetics. Experimental techniques such as *in situ* infrared spectroscopy and *in situ* solid-state NMR can provide dynamic catalytic reaction data under real reaction conditions, enabling the identification and tracking of critical intermediates, as well as the real-time monitoring of reactant-active center interactions. Theoretical methods such as density functional theory and molecular dynamics simulations offer theoretical support for analyzing the MTO reaction mechanism. The application of these techniques will allow for a multidimensional analysis of the molecular sieve catalytic reaction mechanism. By gaining a more comprehensive understanding of the coupled reaction-adsorption–diffusion mechanism, the complex mechanism of catalytic reactions would be revealed, which also contributes to the improvements in catalyst design, the optimization of industrial catalytic processes, and the advancement of green chemistry and sustainable development.

## Data availability

No primary research results, software, or code have been included, and no new data were generated or analysed as part of this feature article.

## Conflicts of interest

There are no conflicts to declare.

## Acknowledgements

This work was supported by the National Key Research and Development Program of China (no. 2022YFE0116000), the National Natural Science Foundation of China (22241801, 22022202, 22032005, 22288101, 21991090, 21991092, and 21991093), the Dalian Outstanding Young Scientist Foundation (2021RJ01), and the Liaoning International Joint Laboratory Project (2024JH2/102100005).

## References

1 X. Zhou, Z. Sun, H. Yan, X. Feng, H. Zhao, Y. Liu, X. Chen and C. Yang, *J. Cleaner Prod.*, 2021, **308**, 127283.
2 C. D. Chang and A. J. Silvestri, *J. Catal.*, 1977, **47**, 249–259.
3 I. Yarulina, A. D. Chowdhury, F. Meirer, B. M. Weckhuysen and J. Gascon, *Nat. Catal.*, 2018, **1**, 398–411.
4 P. Tian, Y. Wei, M. Ye and Z. Liu, *ACS Catal.*, 2015, **5**, 1922–1938.
5 S. Xu, Y. Zhi, J. Han, W. Zhang, X. Wu, T. Sun, Y. Wei and Z. Liu, in *Adv. Catal.*, ed. C. Song, Academic Press, 2017, vol. 61, pp. 37–122.
6 U. Olsbye, S. Svelle, M. Bjørgen, P. Beato, T. V. W. Janssens, F. Joensen, S. Bordiga and K. P. Lillerud, *Angew. Chem., Int. Ed.*, 2012, **51**, 5810–5831.
7 J. Zhong, J. Han, Y. Wei and Z. Liu, *J. Catal.*, 2021, **396**, 23–31.
8 M. Dusselier and M. E. Davis, *Chem. Rev.*, 2018, **118**, 5265–5329.
9 M. Moliner, C. Martínez and A. Corma, *Chem. Mater.*, 2013, **26**, 246–258.
10 P. Ferri, C. Li, C. Paris, A. Vidal-Moya, M. Moliner, M. Boronat and A. Corma, *ACS Catal.*, 2019, **9**, 11542–11551.
11 W. Zhang, S. Lin, Y. Wei, P. Tian, M. Ye and Z. Liu, *Natl. Sci. Rev.*, 2023, **10**, nwad120.
12 N. Wang, Y. Zhi, Y. Wei, W. Zhang, Z. Liu, J. Huang, T. Sun, S. Xu, S. Lin, Y. He, A. Zheng and Z. Liu, *Nat. Commun.*, 2020, **11**, 1079.
13 S. Gao, J. Yuan, Z. Liu, C. Lou, Z. Yu, S. Xu, A. Zheng, P. Wu, Y. Wei and Z. Liu, *J. Phys. Chem. C*, 2021, **125**, 6832–6838.
14 S. Gao, Z. Liu, S. Xu, A. Zheng, P. Wu, B. Li, X. Yuan, Y. Wei and Z. Liu, *J. Catal.*, 2019, **377**, 51–62.
15 S. Xu, A. Zheng, Y. Wei, J. Chen, J. Li, Y. Chu, M. Zhang, Q. Wang, Y. Zhou, J. Wang, F. Deng and Z. Liu, *Angew. Chem., Int. Ed.*, 2013, **52**, 11564–11568.
16 B. P. C. Hereijgers, F. Bleken, M. H. Nilsen, S. Svelle, K.-P. Lillerud, M. Bjørgen, B. M. Weckhuysen and U. Olsbye, *J. Catal.*, 2009, **264**, 77–87.
17 W. Zhang, J. Chen, S. Xu, Y. Chu, Y. Wei, Y. Zhi, J. Huang, A. Zheng, X. Wu, X. Meng, F. Xiao, F. Deng and Z. Liu, *ACS Catal.*, 2018, **8**, 10950–10963.
18 J. Li, Y. Wei, J. Chen, S. Xu, P. Tian, X. Yang, B. Li, J. Wang and Z. Liu, *ACS Catal.*, 2015, **5**, 661–665.
19 J. Liang, H. Li, S. Zhao, W. Guo, R. Wang and M. Ying, *Appl. Catal.*, 1990, **64**, 31–40.
20 M. Yang, B. Li, M. Gao, S. Lin, Y. Wang, S. Xu, X. Zhao, P. Guo, Y. Wei, M. Ye, P. Tian and Z. Liu, *ACS Catal.*, 2020, **10**, 3741–3749.
21 W. Zhang, Y. Zhi, J. Huang, X. Wu, S. Zeng, S. Xu, A. Zheng, Y. Wei and Z. Liu, *ACS Catal.*, 2019, **9**, 7373–7379.
22 X. Li, Q. Sun, Y. Li, N. Wang, J. Lu and J. Yu, *J. Phys. Chem. C*, 2014, **118**, 24935–24940.
23 J. Chen, J. Li, Y. Wei, C. Yuan, B. Li, S. Xu, Y. Zhou, J. Wang, M. Zhang and Z. Liu, *Catal. Commun.*, 2014, **46**, 36–40.
24 I. Pinilla-Herrero, U. Olsbye, C. Márquez-Álvarez and E. Sastre, *J. Catal.*, 2017, **352**, 191–207.
25 J. H. Kang, F. H. Alshafei, S. I. Zones and M. E. Davis, *ACS Catal.*, 2019, **9**, 6012–6019.
26 J. van den Bergh, J. Gascon and F. Kapteijn, in *Zeolites and Catalysis*, ed. J. Čejka, A. Corma and S. Zones, Wiley-VCH Verlag GmbH & Co. KGaA, 2010, pp. 361–387.
27 D. Chen, K. Moljord and A. Holmen, *Microporous Mesoporous Mater.*, 2012, **164**, 239–250.
28 J. Han, Z. Liu, H. Li, J. Zhong, W. Zhang, J. Huang, A. Zheng, Y. Wei and Z. Liu, *ACS Catal.*, 2020, **10**, 8727–8735.
29 D. Selassie, D. Davis, J. Dahlin, E. Feise, G. Haman, D. S. Sholl and D. Kohen, *J. Phys. Chem. C*, 2008, **112**, 16521–16531.
30 G. S. Armatas, *Chem. Eng. Sci.*, 2006, **61**, 4662–4675.
31 A. Ghysels, S. L. C. Moors, K. Hemelsoet, K. De Wispelaere, M. Waroquier, G. Sastre and V. Van Speybroeck, *J. Phys. Chem. C*, 2015, **119**, 23721–23734.

 

32 P. Cnudde, R. Demuynck, S. Vandenbrande, M. Waroquier, G. Sastre and V. V. Speybroeck, *J. Am. Chem. Soc.*, 2020, **142**, 6007–6017.
33 J. Li, Y. Wei, J. Chen, P. Tian, X. Su, S. Xu, Y. Qi, Q. Wang, Y. Zhou, Y. He and Z. Liu, *J. Am. Chem. Soc.*, 2011, **134**, 836–839.
34 W. Rao, X. Tang, K. Lin, X. Xu, H. Xia, Y. Jiang, Z. Liu and A. Zheng, *J. Phys. Chem. Lett.*, 2023, **14**, 3567–3573.
35 Z. Liu, J. Yuan, J. M. van Baten, J. Zhou, X. Tang, C. Zhao, W. Chen, X. Yi, R. Krishna, G. Sastre and A. Zheng, *Sci. Adv.*, 2021, **7**, eabf0775.
36 Z. Liu, J. Zhou, X. Tang, F. Liu, J. Yuan, G. Li, L. Huang, R. Krishna, K. Huang and A. Zheng, *AlChE J.*, 2020, **66**, e16269.
37 C. Lou, W. Zhang, C. Ma, B. Fan, S. Xu, S. Gao, P. Guo, Y. Wei and Z. Liu, *ChemCatChem*, 2021, **13**, 1299–1305.
38 S. Gao, S. Xu, Y. Wei, Z. Liu, A. Zheng, P. Wu and Z. Liu, *Chem. Commun.*, 2019, **55**, 10693–10696.
39 Q. Chen, J. Liu and B. Yang, *Nat. Commun.*, 2021, **12**, 3725.
40 J. Karger and D. M. Ruthven, *Diffusion in Zeolites and Other Microporous Solids*, John Wiley, New York, USA, 1992.
41 S. Al-Khattaf and H. D. Lasa, *Ind. Eng. Chem. Res.*, 1999, **38**, 1350–1356.
42 A. Waghray, R. Oukaci and D. G. Blackmond, *Catal. Lett.*, 1992, **14**, 115–122.
43 J. Liu, G. Jiang, Y. Liu, J. Di, Y. Wang, Z. Zhao, Q. Sun, C. Xu, J. Gao, A. Duan, J. Liu, Y. Wei, Y. Zhao and L. Jiang, *Sci. Rep.*, 2014, **4**, 7276.
44 M. Sun, J. Zhou, Z. Hu, L. Chen, L. Li, Y. Wang, Z. Xie, S. Turner, G. Van Tendeloo, T. Hasan and B. Su, *Matter*, 2020, **3**, 1226–1245.
45 S. Tao, X. Li, X. Wang, Y. Wei, Y. Jia, J. Ju, Y. Cheng, H. Wang, S. Gong, X. Yao, H. Gao, C. Zhang, Q. Zang and Z. Tian, *Angew. Chem., Int. Ed.*, 2020, **59**, 3455–3459.
46 X. Zhu, Y. Gao, H. Chen, M. Jiang, X. Wang, C. Miao, Y. Shen, Y. Ji, Z. Qin, Z. Wu, W. Song, C. Xu and B. Shen, *Angew. Chem., Int. Ed.*, 2024, **63**, e202411446.
47 S. Hu, J. Chen, Q. Zhang, J. Liu, J. Meng, G. Ye, X. Zhou and W. Yuan, *AlChE J.*, 2022, **68**, e17677.
48 M. Albahar, C. Li, V. L. Zholobenko and A. A. Garforth, *Microporous Mesoporous Mater.*, 2020, **302**, 110221.
49 S. Xu, X. Zhang, D. Cheng, F. Chen and X. Ren, *Front. Chem. Sci. Eng.*, 2018, **12**, 780–789.
50 P. Cnudde, E. A. Redekop, W. Dai, N. G. Porcaro, M. Waroquier, S. Bordiga, M. Hunger, L. Li, U. Olsbye and V. Van Speybroeck, *Angew. Chem., Int. Ed.*, 2021, **60**, 10016–10022.
51 R. Krishna and J. M. van Baten, *Sep. Purif. Technol.*, 2008, **61**, 414–423.
52 J. Xiao and J. Wei, *Chem. Eng. Sci.*, 1992, **47**, 1123–1141.
53 J. Kärger, D. M. Ruthven and D. N. Theodorou, *Diffusion in Nanoporous Materials*, Wiley-VCH, 2012.
54 W. Dai, M. Scheibe, L. Li, N. Guan and M. Hunger, *J. Phys. Chem. C*, 2012, **116**, 2469–2476.
55 J. Zhong, J. Han, Y. Wei, S. Xu, Y. He, Y. Zheng, M. Ye, X. Guo, C. Song and Z. Liu, *Chem. Commun.*, 2018, **54**, 3146–3149.
56 J. Zhong, J. Han, Y. Wei, S. Xu, T. Sun, X. Guo, C. Song and Z. Liu, *Chin. J. Catal.*, 2018, **39**, 1821–1831.
57 J. Zhong, J. Han, Y. Wei, S. Xu, T. Sun, X. Guo, C. Song and Z. Liu, *J. Energy Chem.*, 2019, **32**, 174–181.
58 S. Lin, Y. Wei and Z. Liu, *Chem Catal.*, 2023, **3**, 100597.
59 C. Wang, Y. Wang and Z. Xie, *J. Catal.*, 2013, **301**, 8–19.
60 K. Hemelsoet, J. Van der Mynsbrugge, K. De Wispelaere, M. Waroquier and V. Van Speybroeck, *ChemPhysChem*, 2013, **14**, 1526–1545.
61 Y. Wei, C. Yuan, J. Li, S. Xu, Y. Zhou, J. Chen, Q. Wang, L. Xu, Y. Qi, Q. Zhang and Z. Liu, *ChemSusChem*, 2012, **5**, 906–912.
62 D. Mores, E. Stavitski, M. H. F. Kox, J. Kornatowski, U. Olsbye and B. M. Weckhuysen, *Chem. – Eur. J.*, 2008, **14**, 11320–11327.
63 S. Wang, Z. Qin, M. Dong, J. Wang and W. Fan, *Chem. Catal.*, 2022, **2**, 1657–1685.
64 Y. Liu, S. Müller, D. Berger, J. Jelic, K. Reuter, M. Tonigold, M. Sanchez-Sanchez and J. A. Lercher, *Angew. Chem., Int. Ed.*, 2016, **55**, 5723–5726.
65 A. D. Chowdhury, K. Houben, G. T. Whiting, M. Mokhtar, A. M. Asiri, S. A. Al-Thabaiti, S. N. Basahel, M. Baldus and B. M. Weckhuysen, *Angew. Chem., Int. Ed.*, 2016, **55**, 15840–15845.
66 T. Sun, W. Chen, S. Xu, A. Zheng, X. Wu, S. Zeng, N. Wang, X. Meng, Y. Wei and Z. Liu, *Chem*, 2021, **7**, 2415–2428.
67 X. Wu, S. Xu, Y. Wei, W. Zhang, J. Huang, S. Xu, Y. He, S. Lin, T. Sun and Z. Liu, *ACS Catal.*, 2018, **8**, 7356–7361.
68 H. Yamazaki, H. Shima, H. Imai, T. Yokoi, T. Tatsumi and J. N. Kondo, *Angew. Chem., Int. Ed.*, 2011, **50**, 1853–1856.
69 X. Wu, Y. Wei and Z. Liu, *Acc. Chem. Res.*, 2023, **56**, 2001–2014.
70 S. Lin, Y. Zhi, W. Chen, H. Li, W. Zhang, C. Lou, X. Wu, S. Zeng, S. Xu, J. Xiao, A. Zheng, Y. Wei and Z. Liu, *J. Am. Chem. Soc.*, 2021, **143**, 12038–12052.
71 J. Goetze, F. Meirer, I. Yarulina, J. Gascon, F. Kapteijn, J. Ruiz-Martínez and B. M. Weckhuysen, *ACS Catal.*, 2017, **7**, 4033–4046.
72 P. Ferri, C. Li, R. Millán, J. Martínez-Triguero, M. Moliner, M. Boronat and A. Corma, *Angew. Chem., Int. Ed.*, 2020, **59**, 19708–19715.
73 W. Song, J. F. Haw, J. B. Nicholas and C. S. Heneghan, *J. Am. Chem. Soc.*, 2000, **122**, 10726–10727.
74 S. Fan, H. Wang, P. Wang, W. Jiao, S. Wang, Z. Qin, M. Dong, J. Wang and W. Fan, *Chem. Catal.*, 2024, **4**, 100927.
75 S. Gao, S. Xu, Y. Wei, Q. Qiao, Z. Xu, X. Wu, M. Zhang, Y. He, S. Xu and Z. Liu, *J. Catal.*, 2018, **367**, 306–314.
76 S. Lin, Y. Zhi, Z. Liu, J. Yuan, W. Liu, W. Zhang, Z. Xu, A. Zheng, Y. Wei and Z. Liu, *Natl. Sci. Rev.*, 2022, **9**, nwac151.
77 Y. Wei, J. Li, C. Yuan, S. Xu, Y. Zhou, J. Chen, Q. Wang, Q. Zhang and Z. Liu, *Chem. Commun.*, 2012, **48**, 3082–3084.
78 M. Guisnet, L. Costa and F. R. Ribeiro, *J. Mol. Catal. A: Chem.*, 2009, **305**, 69–83.
79 G. J. Yang, Y. X. Wei, S. T. Xu, J. R. Chen, J. Z. Li, Z. M. Liu, J. H. Yu and R. R. Xu, *J. Phys. Chem. C*, 2013, **117**, 8214–8222.
80 K. De Wispelaere, C. S. Wondergem, B. Ensing, K. Hemelsoet, E. J. Meijer, B. M. Weckhuysen, V. Van Speybroeck and J. Ruiz-Martínez, *ACS Catal.*, 2016, **6**, 1991–2002.
81 Q. Peng, G. Wang, Z. Wang, R. Jiang, D. Wang, J. Chen and J. Huang, *ACS Sustainable Chem. Eng.*, 2018, **6**, 16867–16875.